JEMAT, 2025, Vol 13, No 1, 55-65
https://doi.org/10.54987/jemat.v13i1.1112

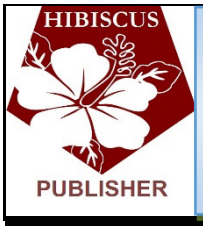

JOURNAL OF ENVIRONMENTAL MICROBIOLOGY AND TOXICOLOGY

Website: http://journal.hibiscuspublisher.com/index.php/JEMAT/index

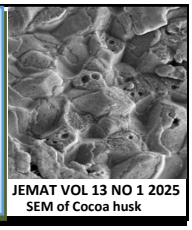

Sugarcane bagasse for the Adsorption of Chromium Ions: Isothermal Remodeling and MOORA-Based Model Selection

Aisha Grema[1], Nur Adeela Yasid[1,2], Mohd Ezuan Khayat[1,2], Mohd Badrin Hanizam Abdul Rahim[1,2], Ain Aqilah Basirun[1,2] and Mohd Yunus Shukor[1,2]*

[1]Department of Biochemistry, Faculty of Biotechnology and Biomolecular Sciences, Universiti Putra Malaysia, 43400 UPM, Serdang, Malaysia.
[2]Agribiotechnology Group, Faculty of Biotechnology and Biomolecular Sciences, Universiti Putra Malaysia, UPM 43400 Serdang, Selangor, Malaysia.

*Corresponding author:
Mohd Yunus Shukor,
Department of Biochemistry,
Faculty of Biotechnology and Biomolecular Sciences,
Universiti Putra Malaysia,
43400 UPM,
Serdang,
Malaysia.
Email: mohdyunus@upm.edu.my

History

Received: 28th March 2025
Received in revised form: 21st May 2025
Accepted: 30th July 2025

Keywords

Chromium (VI) adsorption
Sugarcane bagasse
Isothermal modeling
Nonlinear regression
MOORA ranking

Abstract

This study investigates the adsorption of hexavalent chromium ions (Cr(VI)) onto sugarcane bagasse, employing nonlinear regression to evaluate isothermal models. The experimental data were reanalyzed by converting initial concentrations to equilibrium concentrations (C_e), revealing a monolayer adsorption behavior with a maximum adsorption capacity (Q_m) plateauing at 5.75 mg/g. A series of isotherm models was fitted to the data using nonlinear regression, and performance was assessed using multiple error functions. While most models showed good fits, the Koble-Carrigan, Henry, and Dubinin–Radushkevich models were excluded due to poor convergence or high error. The Multiobjective Optimization on the Basis of Ratio Analysis (MOORA) method was employed for model ranking, identifying the Jovanovic, Toth, Redlich–Peterson and Fritz–Schlunder III models as the top performers. The determined maximum adsorption capacity (Q_{mJ}) based on the Jovanovic isotherm was found to be 5.84 mg/g, which is very close to the experimental maximum (5.75 mg/g) observed in the experimental data. The binding constant (K_{JI} = 0.02 L/mg) indicates that the affinity was weak. The narrow 95% CI indicates a close fit of the model to the raw data. Despite robust modeling, the limited dataset (n = 8) introduces uncertainty in parameter estimation, underscoring the need for larger datasets. This study also emphasizes MOORA's potential in adsorption science as an efficient multi-criteria model selection tool.

INTRODUCTION

Chromium pollution is driven by the rapid industrial growth and the cycling of chromium between its trivalent (Cr(III)) and hexavalent (Cr(VI)) forms, and it remains a pressing global environmental challenge as chromium, especially the hexavalent form is highly toxic and carcinogenic. Industries that deal with metallurgical processing, electroplating, leather tanning, dye production, and steel fabrication is the global chromium main uses, and it is from these industries that, through the release of Cr(VI) through improper waste handling, fugitive emissions, and contaminated effluents, represent the major source of chromium pollution [1]. The anionic chromate/dichromate species are very mobile and represent the toxicity of Cr(VI) in soils and waters. This mobility allows chromium to readily migrate and bioaccumulate, posing risks to aquatic life and human health via ingestion, inhalation, and dermal exposure. The persistence of chromium pollution sources, particularly in areas near mining, electroplating, and industrial zones in developing countries, is attributed to regulatory gaps and uneven monitoring [2]. In Malaysia, industrial estates, electroplating workshops, and leather facilities are major sources of chromium pollution, and is a reflection of a mix of historical and contemporary pressures. Chromium pollution contributes Cr(VI) and Cr(III) to surface waters and sediments, with a disproportionate impact on rural and peri-urban communities through contaminated groundwater and downstream effluents [2].

In Malaysia, elevated chromium concentrations are found in river systems near industrial clusters. This highlights the necessity for robust and improved effluent treatment, more integrated water quality management, and regular monitoring to

safeguard ecosystems and public health [2]. The toxicity of chromium is species-dependent. Cr(III) is less toxic due to its limited water solubility; however, it is essential in trace amounts as a cofactor of enzymes, but becomes hazardous at elevated exposure levels. On the other hand, Cr(VI) species have strong oxidative capabilities and have the ability to cross cell membranes. This makes this species highly toxic, mutagenic, and carcinogenic. Long-term exposure to Cr(VI) can lead to respiratory problems, kidney damage, and developmental effects, highlighting the need for more stringent standards for discharge and lifecycle risk assessments in its remediation [1].
The ongoing demand for chromium in steel alloys, corrosion-resistant coatings, and tanning agents has created a paradox: it is essential for modern industry, but at the same time, it also presents substantial environmental trade-offs when found at excessive levels in the environment. This issue has motivated researchers to shift toward sustainable practices, which include more advanced treatment technologies and holistic, circular approaches to manage or remediate chromium pollution and waste [3].

Chromium remediation techniques include chemical reduction, electrochemical treatment, precipitation, ion exchange, and bioremediation. Among these methods, biosorption—utilizing natural or engineered biological materials as adsorbents to remove Cr(VI) from polluted environments—offers several prominent benefits, including low operating costs, compatibility with low-energy processes, and the potential for regenerating and reusing adsorbents. These advantages make it particularly attractive in developing and underdeveloped countries [4–7].

The premise of biosorption as the best method in environmental friendliness and cost are due to several advantages: (1) economic feasibility since its processing uses simple process requirements and it is also a low-cost feedstocks; (2) compared with physico-chemical methods, biosortpion is considered a reduced energy consumption process; (3) biosorption uses minimal chemical additives and also minimal waste generation; and (4) it has a potential for recycling of adsorbent, and also metal recovery, which enables a circular use of chromium resources. Biosorption aligns well with the UN's Sustainable Development Goals by preserving ecosystem integrity, leveraging waste materials, and offering scalable solutions—in Malaysia and beyond, through pilot plants and decentralized treatment systems [8,9].

In Malaysia, agricultural biomass such as sugarcane bagasse (SB) is increasingly recognized as a highly cost-effective adsorbent for removing xenobiotics, including heavy metals like chromium, from wastewater. In Malaysia, chromium biosorption using agricultural byproducts e.g., tea waste (TW), coconut shell (CS), orange peel (OP) [5] rice husk carbon [10], coconut coir [4], coconut husk [6], *Ananas comosus* (AC) peel, *Parkia speciosa* (PS) pods and *Psidium guajava* (PG) peel [11], including sugarcane bagasse [12].

Sugarcane cultivation is historically an extensively cultivated agricultural commodity in Malaysia, and the resulting bagasse is abundantly available and inexpensive to procure, often treated as agricultural waste. This makes SB an ideal for low-cost environmental remediation strategies. SB possesses reactive functional groups, high surface area, and adequate porosity that can enhance its adsorption capacity for toxicants such as Cr(VI), dyes, and antibiotics [12–19]. The use of SB in biosorption of pollutants aligns with Malaysia's sustainability goals by valorizing agricultural waste and minimizing landfill use. The synergy between economic feasibility, protection of the environment, and circular economy makes sugarcane bagasse a premier adsorbent for xenobiotic removal in the Malaysian context. In this work, the adsorption of chromium on sugarcane bagasse is modeled using various isotherms, and the best model is selected based on MOORA analysis.

METHODS

Data acquisition and fitting

Figure 4b data from a previously published study [13] was digitized using the freeware Webplotdigitizer 2.5 [20]. The program's digitization capabilities have garnered accolades for their reliability [21]. Then, Curve-Expert Professional (Version 2.6.5, copyright Daniel Hyams), a program for curve fitting, was used to perform nonlinear regression on the data. MATLAB software package (Mathworks, Massachusetts, USA) was used to resolve the implicit equations.

Isotherms

Due to the low number of data points, only models (**Table 1**) with parameters limited to three were deemed appropriate to prevent overfitting.

Statistical analysis

This study employed the following statistical discriminatory or error functions tests; HQ (Hannan and Quinn's Criterion) [22], Bias Factor (BF), Accuracy Factor (AF) [23], root-mean-squared error (RMSE), adjusted coefficient of determination (R^2) [24], corrected Akaike Information Criterion (AICc) [25,26], Marquardt's percent standard deviation (MPSD) [27–29] and Bayesian Information Criterion (BIC) [30]. In general, n is the total number of observations, *Obi* and *Pdi* are the predicted and observed values, and p is the total number of parameters of the model [31].

RMSE was calculated using the following formula;

$$RMSE = \sqrt{\frac{\sum_{i=1}^{n}(Pd_i - Ob_i)^2}{n-p}} \quad \text{(Eqn. 1)}$$

BF and AF were calculated using the following formula;

$$Bias\ factor = 10\left(\sum_{i=1}^{n} log\frac{(Pd_i/Ob_i)}{n}\right) \quad \text{(Eqn. 2)}$$

$$Accuracy\ factor = 10\left(\sum_{i=1}^{n} log\frac{|(Pd_i/Ob_i)|}{n}\right) \quad \text{(Eqn. 3)}$$

AICc was calculated using the following formula;

$$AICc = 2p + n\ln\left(\frac{RSS}{n}\right) + \frac{2(p+1)+2(p+2)}{n-p-2} \quad \text{(Eqn. 4)}$$

BIC was calculated using the following formula;

$$BIC = n\ln\left(\frac{RSS}{n}\right) + k\ln(n) \quad \text{(Eqn. 5)}$$

HQC was calculated using the following formula;

$$HQC = nIn\left(\frac{RSS}{n}\right) + 2k\ln(\ln n) \quad \text{(Eqn. 6)}$$

Adjusted coefficient of determination (R^2) was calculated using the following formula;

$$Adjusted\ (R^2) = 1 - \frac{RMS}{S_Y^2} \quad \text{(Eqn. 7)}$$

$$Adjusted\ (R^2) = 1 - \frac{(1-R^2)(n-1)}{(n-p-1)} \quad \text{(Eqn. 8)}$$

MPSD was calculated using the following formula;

$$MPSD = 100\sqrt{\frac{1}{n-p}\sum_{i=1}^{n}\left(\frac{Ob_i - Pd_i}{Ob_i}\right)^2} \quad \text{(Eqn. 9)}$$

Table 1. Mathematical models in the remodelling data [32,33].

Isotherm	p	Formula	Ref.
Henry's law	1	$q_e = HC_e$	[34]
Langmuir	2	$q_e = \frac{q_{mL} b_L C_e}{1 + b_L C_e}$	[32]
Jovanovic	2	$q_e = q_{mJ}(1 - e^{-K_J C_e})$	[35]
Freundlich	2	$q_e = K_F C_e^{\frac{1}{n_F}}$	[36]
Dubinin-Radushkevich[a]	2	Incorrect form $q_e = q_{mDR} exp\left\{-K_{DR}\left[RTln\left(1+\frac{1}{C_e}\right)\right]^2\right\}$ correct form $q_e = q_{mDR} exp\left\{-K_{DR}\left[RTln\left(\left(\frac{C_s}{C_e}\right)\right)\right]^2\right\}$	[37,38] [39,40]
Koble-Corrigan[c]	3	$q_e = \frac{AC_e^n}{1 + BC_e^n}$	[41]
Temkin[a]	3	$q_e = \frac{RT}{b_T}\{ln(a_T C_e)\}$	[42,43]
Redlich-Peterson	3	$q_e = \frac{K_{RP1} C_e}{1 + K_{RP2} C_e^{\beta_{RP}}}$	[44]
Sips[c]	3	$q_e = \frac{K_S q_{mS} C_e^{\frac{1}{n_S}}}{1 + K_S C_e^{\frac{1}{n_S}}}$	[45]
Toth	3	$q_e = \frac{q_{mT} C_e}{\left(K_T + C_e^{n_T}\right)^{n_T}}$	[46]
Hill[c]	3	$q_e = \frac{q_{mH} C_e^{n_H}}{K_H + C_e^{n_H}}$	[47]
Khan	3	$q_e = \frac{q_{mK} b_K C_e}{(1 + b_K C_e)^{a_K}}$	[48]
BET	3	$q_e = \frac{q_{mBET} \alpha_{BET} C_e}{(1 - \beta_{BET} C_e)(1 - \beta_{BET} C_e + \alpha_{BET} C_e)}$	[49]
Vieth-Sladek	3	$q_e = \frac{q_{mVS} b_{VS} C_e}{(1 + b_{VS} C_e)^{n_{VS}}}$	[50]
Radke-Prausnitz	3	$q_e = \frac{A_{RP} B_{RP} C_e^{\beta}}{A_{RP} + B_{RP} C_e^{\beta - 1}}$	[51–53]
Brouers–Sotolongo	3	$q_e = q_{mBS}\left[1 - \left(1 + (0.5)\left(\frac{t}{\tau}\right)^{\alpha}\right)^{-2}\right]$	[54–56]
Fritz-Schlunder-III	3	$q_e = \frac{q_{mFS} K_{FS} C_e}{1 + K_{FS} C_e^{n_{FS}}}$	[57]
Fowler-Guggenheim[a,b]	3	$q_e = q_{mFG} \frac{K_L C_e e^{\frac{\alpha q_e}{q_{mFG}}}}{1 + K_L C_e e^{\frac{\alpha q_e}{q_{mFG}}}}$	[58]
Moreau	3	$q_e = q_{mM} \frac{bC_e + lb^2 C_e^{\,2}}{1 + 2bC_e + lb^2 C_e^{\,2}}$	[59]
Unilan	3	$q_e = \frac{q_{mU}}{2b_U} ln\left(\frac{a_U + C_e e^{b_U}}{a_U + C_e e^{-b_U}}\right)$	

Note
[a]Models that include ln(C_e), implicit equation or any logarithmic function involving C_e will fail or produce NaN (undefined) results when $C_e = 0$. Therefore, data points where $C_e = 0$ should be excluded from the analysis.
[b]Implicit equation or function.
[c]The Hill, Liu (omitted), Sips, and Koble–Corrigan isotherm models will be presented in their traditional forms to preserve their historical context and conceptual distinctions, despite their underlying equality [60,61].

Application of Multiobjective Optimization by Ratio Analysis (MOORA) in Modeling

The Multiobjective Optimization by Ratio Analysis (MOORA) was employed for multi-criteria decision-making (MCDM) in the modeling exercise since a mixture of error function superiority is often found for the top models. This approach facilitates the selection of the optimal model by simultaneously evaluating multiple performance metrics [62,63]. The methodology consists of the first step, which is the normalization of the decision matrix to ensure comparability among different performance metrics. The decision matrix was then normalized. Given that these metrics may have varying units and magnitudes, normalization needs to be carried out using the following equation:

$$X'_{ij} = \frac{x_{ij}}{\sqrt{\sum_{i=1}^{n} x_{ij}^2}} \quad \text{(Eqn. 10)}$$

Where X_{ij} is the original value of the j^{th} metric for the i^{th} model, and $X^{'}_{ij}$ is the normalized value**.**

Ratio System Analysis

The normalized values were then aggregated using a ratio system approach. Beneficial criteria (those that should be maximized, $adjR^2$) were summed up, while non-beneficial criteria (the rest of the error functions) or those that should be minimized were subtracted using the following formula:

$$Y_i = \sum_{beneficial} X'_{ij} - \sum_{non-beneficial} X'_{ij} \quad \text{(Eqn. 11)}$$

Where Y_i is the final score for the i^{th} model

In circumstances where certain criteria were deemed more crucial than others, weighted ratios are recommended to be incorporated into the analysis. The suggestion for incorporating Weighted Ratios is not carried out at this point in time, as the consensus on which error functions listed above have priority over the others has not been documented in the literature. The final step is ranking models based on their aggregated performance scores. Higher scores indicated superior performance. The model with the highest value was considered the most optimal based on the given decision criteria. This methodology allowed for an objective and systematic comparison of kinetic models, facilitating the identification of the best-performing model while considering multiple performance metrics simultaneously.

RESULTS AND DISCUSSION

Several models were applied to the equilibrium data of Garg et al. (2007) using nonlinear regression. Data from the publication was converted to the standard C_e instead of the initial concentration.

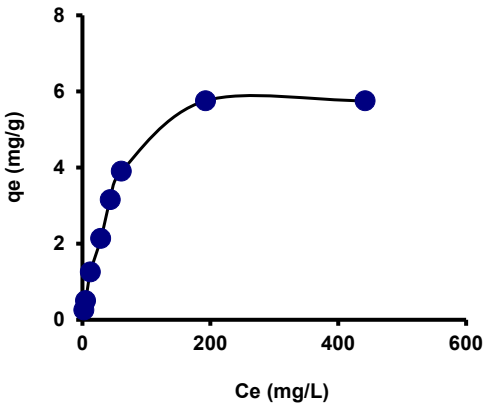

Fig. 1. Equilibrium adsorption of chromium to sugarcane bagasse.

What can be observed from the experimental adsorption data is that the equilibrium adsorption capacity (Q_e) increases with increasing equilibrium concentration (C_e) until a plateau is reached. At low Cr (VI) concentrations (2.5–61 mg/L), the Q_e

was found to rise almost linearly from 0.25 to 3.90 mg/g, indicating a strong initial affinity of the sugarcane bagasse surface for Cr(VI). Beyond the value of C_e = 192.5 mg/L, Q_e was observed to reach a maximum value of 5.75 mg/g. This suggests that a saturation of available binding sites has occurred. This plateau indicates the finite number of adsorption sites, which is typical of a monolayer adsorption process. The fitting of the various isotherms is shown in **Figs**. **2–20**, where all of these models were found to show good data fits, with the exception of the Koble-Carrigan, Henry, and the Dubinin–Radushkevich model, of which the latter failed to converge. Based on the error function analysis shown in **Table 2.** The Multiobjective Optimization on the Basis of Ratio Analysis (MOORA) approach was employed to compare the effectiveness of the adsorption isotherm models, as presented in **Table 3**. The top five models in descending order were found to be the Jovanovic, Toth, Redlich-Peterson, Fritz-Schlunder III and Khan (sharing the spot with Vieth-Sladek and Radke Prausnitz) in descending order, while both Hill, and Sips models shared the same ranked in the form of the SCO or the Standard Competition Order (1-2-2-4), where when two ranks are tied, they received the same rank and the next rank will be skipped one rank [61,64]

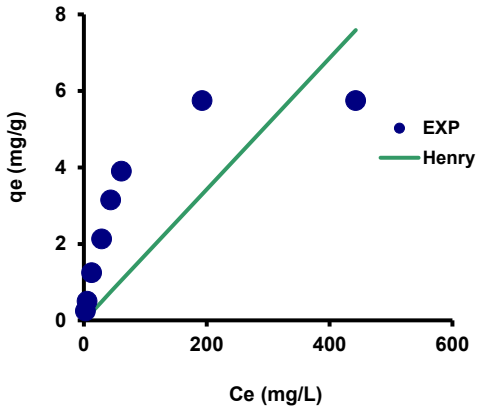

Fig. 2. Cr (VI) adsorption onto sugarcane bagasse modelled using the Henry model.

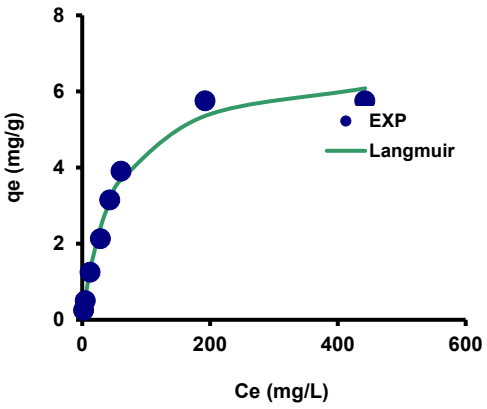

Fig. 3. Cr (VI) adsorption onto sugarcane bagasse modelled using the Langmuir isotherm model.

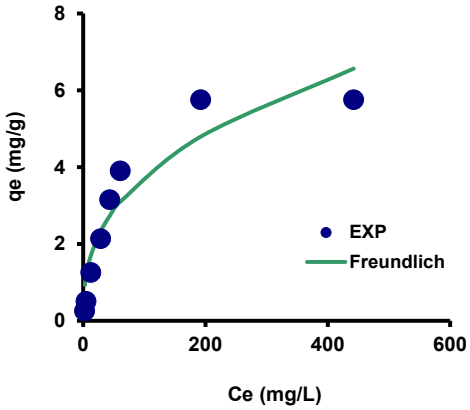

Fig. 4. Cr (VI) adsorption onto sugarcane bagasse modelled using the Freundlich isotherm model.

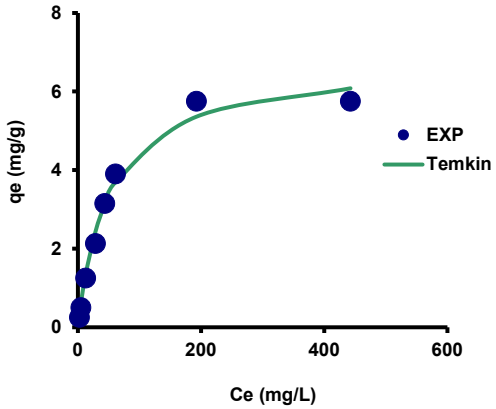

Fig. 5. Cr (VI) adsorption onto sugarcane bagasse modelled using the Temkin isotherm model.

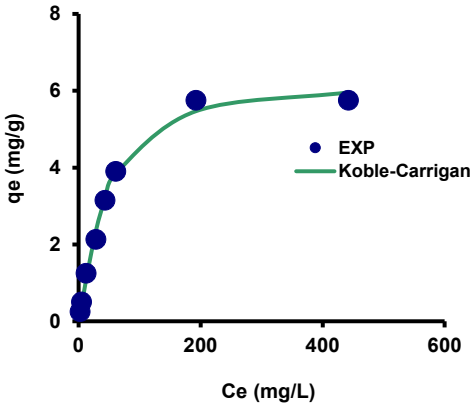

Fig. 6. Cr (VI) adsorption onto sugarcane bagasse modelled using the Koble-Corrigan isotherm model.

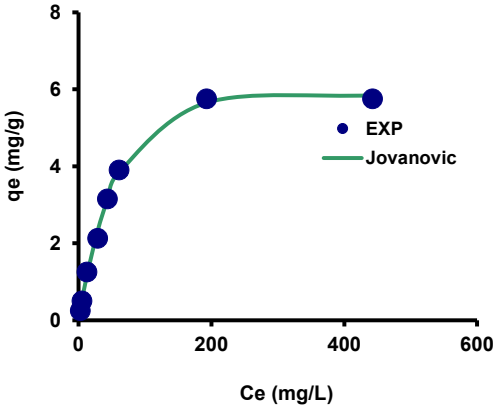

Fig. 7. Cr (VI) adsorption onto sugarcane bagasse modelled using the Jovanovic isotherm model.

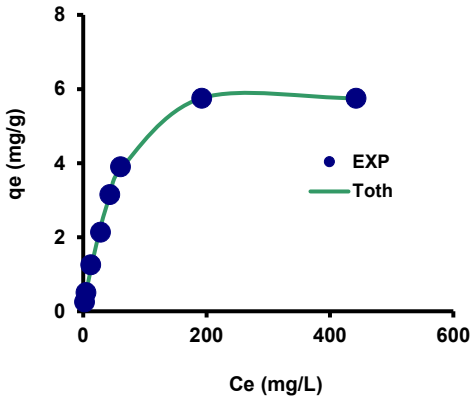

Fig. 10. Cr (VI) adsorption onto sugarcane bagasse modelled using the Toth isotherm model.

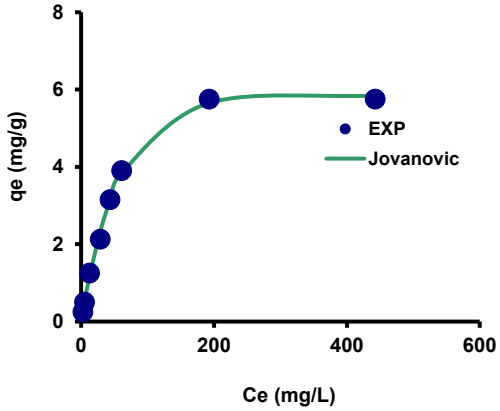

er

Fig. 8. Cr (VI) adsorption onto sugarcane bagasse modelled using the Redlich-Peterson isotherm model.

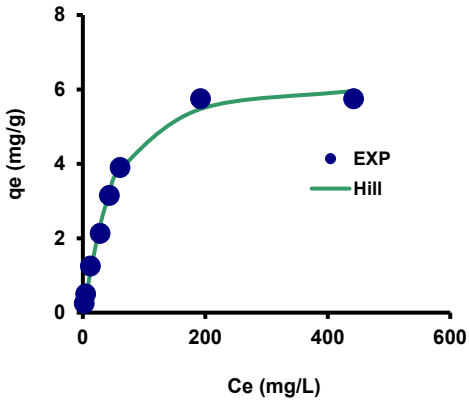

Fig. 11. Cr (VI) adsorption onto sugarcane bagasse modelled using the Hill isotherm model.

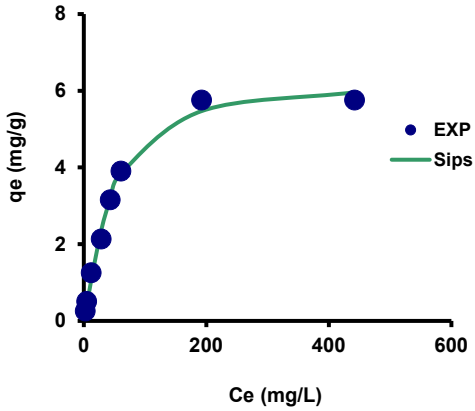

Fig. 9. Cr (VI) adsorption onto sugarcane bagasse modelled using the Sips isotherm model.

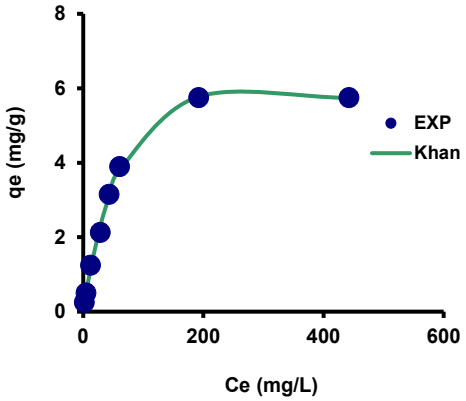

Fig. 12. Cr (VI) adsorption onto sugarcane bagasse modelled using the Khan isotherm model.

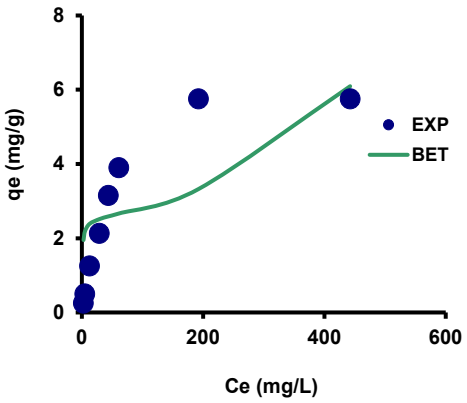

Fig. 13. Cr (VI) adsorption onto sugarcane bagasse modelled using the BET isotherm model.

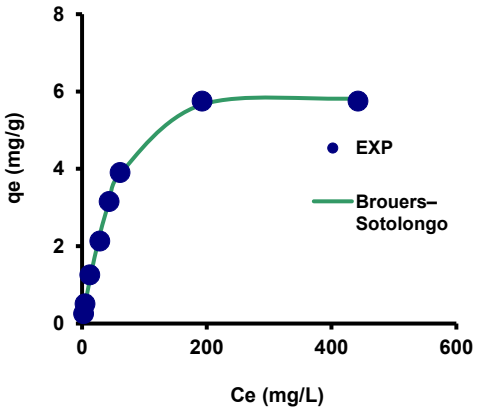

Fig. 16. Cr (VI) adsorption onto sugarcane bagasse modelled using the Brouers-Sotolongo isotherm model.

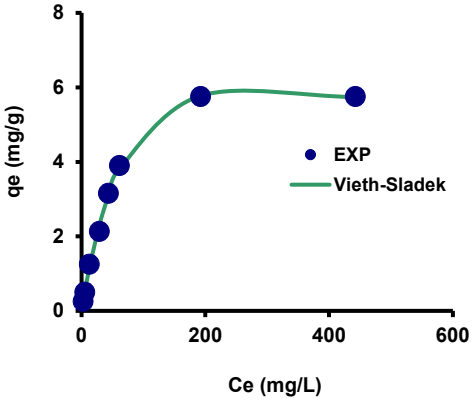

Fig. 14. Cr (VI) adsorption onto sugarcane bagasse modelled using the Vieth-Sladek isotherm model.

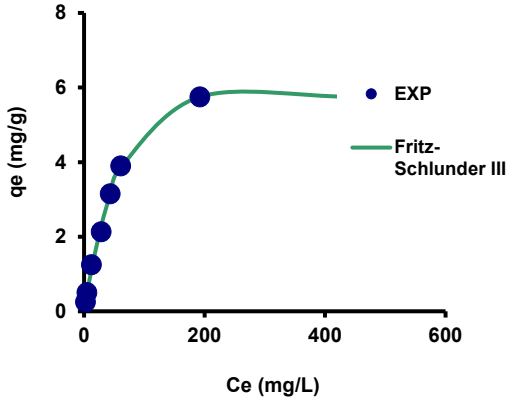

Fig. 17. Cr (VI) adsorption onto sugarcane bagasse modelled using the Fritz-Schlunder III isotherm model.

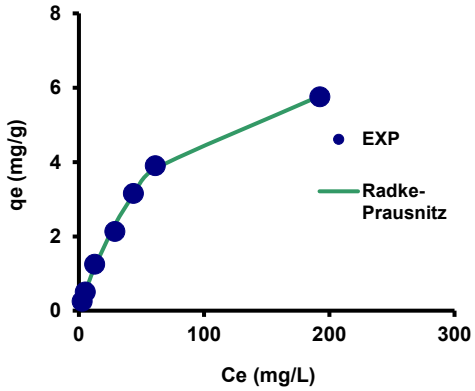

Fig. 15. Cr (VI) adsorption onto sugarcane bagasse modelled using the Radke-Prausnitz isotherm model.

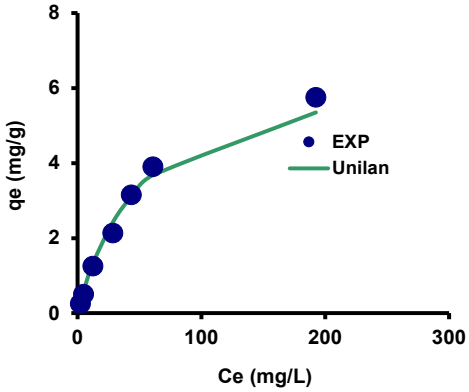

Fig. 18. Cr (VI) adsorption onto sugarcane bagasse modelled using the Unilan isotherm model.

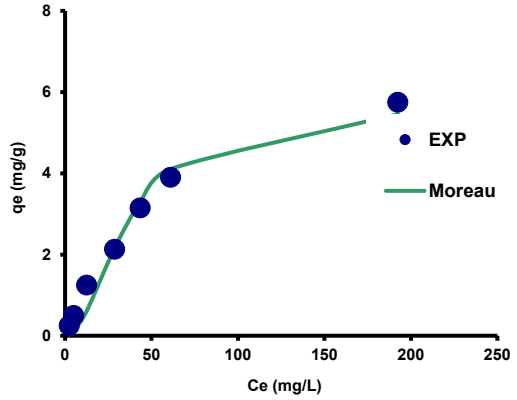

Fig. 19. Cr (VI) adsorption onto sugarcane bagasse modelled using the Moreau isotherm model.

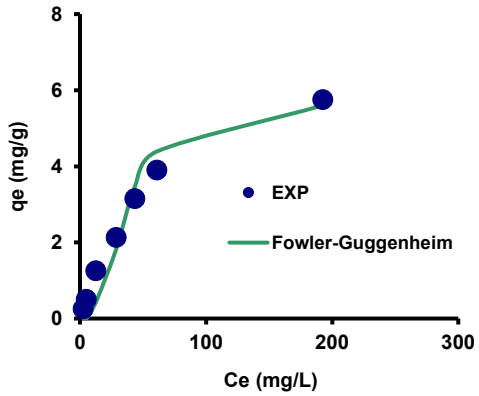

Fig. 20. Cr (VI) adsorption onto sugarcane bagasse modelled using the Fowler-Guggenheim isotherm model.

Table 2. Error function analysis for the fitting of the isotherm of Cr (VI) adsorption onto sugarcane bagasse.

	Model	*p*	MPSD	RMSE	R^2	adR^2	AICc	BIC	HQC	BF	AF
1	Henry	1	197.317	1.973	0.428	0.332	18.21	11.89	11.27	0.46	2.35
2	Langmuir	2	26.583	0.266	0.987	0.981	-7.50	-19.34	-20.57	1.01	1.05
3	Freundlich	2	77.344	0.773	0.860	0.804	9.59	-2.25	-3.48	1.00	1.15
4	Temkin	3	29.122	0.291	0.987	0.976	3.83	-17.26	-19.11	1.01	1.05
5	Koble-Carrigan	2	315.291	0.196	0.428	0.199	-12.34	-24.18	-25.41	0.99	1.05
6	Jovanovic	2	10.561	0.106	0.998	0.997	-22.27	-34.11	-35.34	1.00	1.03
7	Redlich-Peterson	3	9.774	0.098	0.999	0.998	-13.63	-34.73	-36.58	0.99	1.03
8	Sips	3	21.515	0.215	0.993	0.988	-1.01	-22.10	-23.95	0.99	1.05
9	Toth	3	9.725	0.097	0.999	0.998	-13.71	-34.81	-36.66	0.99	1.03
10	Hill	3	21.515	0.215	0.993	0.988	-1.01	-22.10	-23.95	0.99	1.05
11	Khan	3	9.944	0.099	0.999	0.997	-13.36	-34.45	-36.30	1.00	1.02
12	BET	3	173.385	1.734	-0.222	-1.138	32.38	11.28	9.44	0.97	1.28
13	Vieth-Sladek	3	9.944	0.099	0.999	0.997	-13.36	-34.45	-36.30	1.00	1.02
14	Radke-Prausnitz	3	9.944	0.099	0.999	0.997	-13.36	-34.45	-36.30	1.00	1.02
15	Brouers–Sotolongo	3	11.160	0.112	0.998	0.997	-11.51	-32.61	-34.45	0.99	1.03
16	Fritz-Schlunder III	3	9.776	0.098	0.999	0.998	-13.63	-34.73	-36.57	0.99	1.03
17	Unilan	3	29.610	0.296	0.986	0.976	4.10	-16.99	-18.84	1.02	1.05
18	Fowler-Guggenheim	3	54.582	0.546	0.960	0.930	13.89	-7.21	-9.05	0.88	0.88
19	Moreau	3	39.337	0.393	0.980	0.965	8.65	-12.45	-14.30	0.92	0.92

Note:
RMSE Root mean Square Error
adR^2 Adjusted Coefficient of determination
p no of parameters
AF Accuracy factor
BF Bias factor
BIC Bayesian Information Criterion
AICc Adjusted Akaike Information Criterion
HQC Hannan–Quinn information criterion

Table 3. Ranking of isothermal models based on MOORA.

No	Model	MOORA Score	Rank
1	Jovanovic	1.43735	1
2	Toth	1.31919	2
3	Redlich-Peterson	1.31549	3
4	Fritz-Schlunder III	1.31543	4
5	Khan	1.30642	5
6	Vieth-Sladek	1.30642	5
7	Radke-Prausnitz	1.30642	5
8	Brouers–Sotolongo	1.23483	8
9	Langmuir	0.83680	9
10	Sips	0.81234	10
11	Hill	0.81234	10
12	Temkin	0.60365	12
13	Unilan	0.59130	13
14	Moreau	0.38048	14
15	Fowler-Guggenheim	0.09942	15
16	Koble-Carrigan	0.01442	16
17	Freundlich	-0.13409	17
18	Henry	-1.81516	18
19	BET	-2.07700	19

The Jovanovic isotherm assumes a limited quantity of uniform adsorption sites that are devoid of the lateral interaction effect. The determined maximum adsorption capacity (Q_{mJ}) was found to be 5.84 mg/g, which is very close to the experimental maximum (5.75 mg/g) observed in the experimental data. The binding constant (K_{JI} = 0.02 L/mg) indicates that the affinity was weak. The narrow 95% CI indicates a close fit of the model to the raw data (**Table 4**). The Langmuir model also assumes a monolayer adsorption site. The observed maximum adsorption capacity (Q_{mS} = 6.79 mg/g) was found to slightly overestimate the experimental plateau, implying moderate binding based on the low Langmuir constant (k_L = 0.02 L/mg) (**Table 4**).

The Redlich–Peterson model, gave parameters k_{RP1} (L/g) = 0.10, k_{RP2} (L/mg)/g) = 0.0001, and BRP = 1.28. The isotherm combines features of both Langmuir and the Freundlich isotherms. The value of the exponent BRP, which is close to unity, indicates the system trends toward Langmuir-like behavior. This is evident from the experimental data. The flexibility of this model allows fitting across the full C_e range (**Table 4**). The Toth model accounts for heterogeneity in adsorption sites.

The estimated maximum adsorption capacity for the Toth model was 64.04 mg/g, and when compared to the experimental maximum value of 5.75 mg/g suggested that the value was unrealistically high. In addition, coupled with the wide confidence interval (−4.95 to 133.0) (**Table 4**), this indicates that the Toth model is not suited for this dataset, which may be due to the limited heterogeneity of adsorption sites in sugarcane bagasse for Cr(VI). Furthermore, the near unity for the exponent nT (1.107) indicates a nearly homogeneous site distribution, which also points toward Langmuir-type behavior. The raw data and fitted constants collectively indicate that Cr(VI) adsorption onto sugarcane bagasse may follow a monolayer adsorption pattern with a moderate binding affinity.

The Jovanovic and Langmuir models provide good estimates of the maximum adsorption capacity, aligning closely with the experimental value of 5.75 mg/g. Furthermore, the Redlich–Peterson model also fits well, and this reinforces the Langmuir-like nature of the process. A caveat to all of these interpretations is that the number of datasets needs to be very high, close to 15 or more, to be reliable. However, most reports on the interpretation of isothermal modelling rarely have datasets with more than 8 samples, which is a common issue in adsorption research.

Table 4. Isothermal models' constants for Cr (VI) adsorption onto sugarcane bagasse.

Model	Parameter	Value	95% CI Lower	95% CI Upper
Jovanovic	Qm_J (mg/g)	5.84	5.64	6.05
	K_{J1}	0.02	0.01	0.02
Langmuir	Qm_S (mg/g)	6.79	6.09	7.56
	k_L (L/mg)	0.02	0.01	0.02
Redlich-Petersen	k_{RP1} (L/g)	0.10	0.084	0.11
	k_{RP2} (L/mg)/g)	0.0001	0.0004	0.05
	B_{RP}	1.28	1.15	1.39
Toth	q_{mT} (mg g^{-1})	64.04	-4.95 to 133.0	64.04
	K_T $(mg/L)^{nT}$	259.11	87.84 to 430.37	259.11
	n_T	1.107	1.09 to 1.24	1.107

MOORA standardizes performance ratings across criteria and is also characterized by its simplicity and computational efficiency, thereby obviating the need for intricate pairwise comparisons or distance computations. The use of MOORA facilitates clear and swift assessment through the management of criteria with varying units and scales via structured normalization. In various model ranking tasks, MCDM has been successfully and widely utilized, including the assessment of Software Reliability Growth Models (SRGMs) [65], however, its application in adsorption model selection remains scarce [61].

The MOORA score, when calculated to seven decimal places, yields identical values for both the Hill and Sips models, reinforcing the notion that these two models are numerically equivalent. [60] demonstrated that the Hill and Sips models are structurally the same. The application of MOORA for ranking models based on multiple error functions in the adsorption field is expected to increase, as more studies have reported the use of several error functions in addition to the classical coefficient of determination (R^2). For example, in the studies on CO_2 adsorption onto activated carbon, the use of error functions such as the coefficient of determination (R^2), error sum of squares (ERRSQ/SSE), average relative error (ARE), chi-square test (χ^2), hybrid fractional error function (HYBRID), Marquardt's percent standard deviation (MPSD), and error of average bias (EABS) were employed as error functions to find the best model. The authors demonstrate that the HYBRID model is the best, achieving a better fit than the Langmuir isotherm in six out of the eight error functions evaluated [66]. In this scenario, the use of MOORA would be beneficial in assessing the rank.

A notable constraint of nonlinear modeling is that limited datasets (like the eight data points utilized in this study) may inadequately represent adsorption behavior as discussed above. An insufficient dataset increases the chances of recording random noise instead of recognizing authentic adsorption patterns. This often results in overfitting and unreliable parameter estimation of adsorption models, as well as incorrect interpretation of the mechanisms of adsorption. Limited datasets reduce statistical power and causes wide confidence intervals. To address these challenges, resampling techniques such as bootstrapping, Monte Carlo simulations, and sensitivity analysis can be employed to enhance model robustness, leading to greater insight into adsorption behavior [67].

Jovanovic isotherm

The Jovanovic isotherm model assumes adsorption occurs through the formation of a monolayer on a homogeneous adsorbent surface, and in this manner, it is a specialized adsorption isotherm, similar to the Langmuir model. However, the model obviates the need for lateral interactions between adsorbed molecules. One distinctive feature of the Jovanovic isotherm is that it takes into account of surface binding vibrations of the adsorbed species. Hence, this aspect acknowledges the dynamic nature of the adsorbed molecules, where the adsorbate exhibits vibrational movements even when interacting with the adsorption sites. The inclusion of surface binding vibrations introduces a more holistic view of the adsorption process, recognizing that adsorbed molecules are subject to vibrational energy states and are not entirely static. By taking this overview, the outcome is a tie-in to adsorption energy, and therefore, affects the adsorption capacity and kinetics [35].

Toth

The Toth isotherm is a three-parameter model that preserves the correct low- and high-concentration limits, and captures adsorption on energetically heterogeneous surfaces. In the equation, t quantifies heterogeneity, where t→1 results in the Langmuir isotherm, and a smaller t value indicates stronger heterogeneity. It remains physically meaningful over wide ranges and reproduces Henry's law at low C_e values. In several studies, Toth frequently outperforms Langmuir and Sips for dyes and organics, reflecting the model's ability to accommodate broad site-energy distributions while maintaining the monolayer capacity approach [68,69].

Redlich–Peterson model

The Redlich–Peterson (RP) isotherm interpolates between Langmuir and Freundlich behavior, and is a flexible three-parameter equation, making it useful for heterogeneous surfaces. The heterogeneity exponent γ lies between 0 and 1 in the model. The RP reduces to Langmuir when γ = 1, with an apparent monolayer capacity. On the other hand, at low C_e it follows Henry's law. Due to the correlation of its two parameters, nonlinear regression should be performed over the linearized forms. The model is hailed as a benchmark for the three-parameter model, and is widely recommended [70–75].

Langmuir isotherm

The Langmuir isotherm describes adsorption that occurs only when the adsorbent has a uniform structure, resulting in the monolayer adsorption of an adsorbate onto a homogeneous adsorbent surface. In the model, all adsorption sites are identical and have the same energy [76]. The isotherm model is distinct from Henry's law but is related in its foundational principles. Once a single layer of adsorbate molecules fully covers the surface, it is postulated that no further adsorption can occur at those sites, reinforcing the idea of monolayer coverage [71]. The model has been successfully utilized as the best model in modelling equilibrium adsorption of chromium to adsorbents [77–90].

Freundlich isotherm

The Freundlich isotherm model offers a more flexible approach to describing adsorption phenomena, despite it being an empirical equation. The model is suitable in systems with a heterogeneous adsorbent surface where adsorption can occur through multiple layers [91,92]. Unlike the Langmuir isotherm, which assumes uniform adsorption sites and monolayer coverage, the Freundlich isotherm accounts for variations in adsorption site affinities and the potential for multilayer adsorption. One major limitation of the Freundlich equation is its inability to predict the maximum possible adsorption [93]. In addition, it is a more empirical model than a mechanical one. By using the Halsey rearrangement of the Freundlich equation, we can estimate Qm by leveraging the last C_e data point as an approximation for the maximum adsorption capacity.

$$K_F = \frac{q_{mF}}{C_e^{\frac{1}{n_F}}} \qquad \text{(Eqn. 12)}$$

In the equation, it can be observed that the term *Qe* has now been altered to Qm_F.

CONCLUSION

Using various modeling exercises, the adsorption of Cr(VI) onto sugarcane bagasse has demonstrated characteristics that are consistent with monolayer behavior. This is evident from the saturation of adsorption capacity at high equilibrium concentrations. Leveraging the use of nonlinear regression instead of the often-popular linearized forms has provided accurate fits for most models, with 95% confidence interval output. The Jovanovic, Redlich–Peterson, and Toth isotherms align closely with the experimental maximum capacity. The application of the MOORA method for ranking models has introduced a structured, unbiased ranking approach, which has effectively managed the multiple error criteria utilized in this study. MOORA is able to identify models with the highest statistical reliability, while also simplifying and automating decision-making through its computational efficiency. Despite this, the small dataset size remains a limitation in not only this study but also in others in general, which may introduce statistical noise and produce wide confidence intervals that can compromise the estimation of the parameters. In order to address this issue, future studies are encouraged to incorporate larger datasets, preferably larger than 15, and the use of resampling techniques such as bootstrapping or Monte Carlo simulation, which can enhance robustness. To conclude, this study concurs with the suitability of Langmuir-like isotherms for Cr(VI) adsorption onto sugarcane bagasse but also supports MOORA as a valuable tool in adsorption model selection.

REFERENCES

1. Tumolo M, Ancona V, De Paola D, Losacco D, Campanale C, Massarelli C, et al. Chromium Pollution in European Water, Sources, Health Risk, and Remediation Strategies: An Overview. Int J Environ Res Public Health. 2020 Jan;17(15):5438.
2. Mohammadpour A, Gharehchahi E, Gharaghani MA, Shahsavani E, Golaki M, Berndtsson R, et al. Assessment of drinking water quality and identifying pollution sources in a chromite mining region. J Hazard Mater. 2024 Dec 5;480:136050.
3. Prasad S, Yadav KK, Kumar S, Gupta N, Cabral-Pinto MMS, Rezania S, et al. Chromium contamination and effect on environmental health and its remediation: A sustainable approaches. J Environ Manage. 2021 May 1;285:112174.
4. Chaudhuri M, Azizan NKB. Adsorptive Removal of Chromium(VI) from Aqueous Solution by an Agricultural Waste-Based Activated Carbon. Water Air Soil Pollut. 2012 May 1;223(4):1765–71.
5. Amir A, Rahim R, Abdul-Talib S. Removal of Chromium Hexavalent Using Agriculture Waste. Int J Environ Sci Dev. 2017 Jan 1;8:260–3.
6. Hanafiah SFM, Salleh NFM, Ghafar NA, Shukri NM, Kamarudin NHN, Hapani M, et al. Efficiency of Coconut Husk as Agricultural Adsorbent in Removal of Chromium and Nickel Ions from Aqueous Solution. IOP Conf Ser Earth Environ Sci. 2020 Dec;596(1):012048.
7. Konradt N, Dillmann S, Becker J, Schroden D, Rohns HP, Wagner C, et al. Removal of Chromium Species from Low-Contaminated Raw Water by Different Drinking Water Treatment Processes. Water. 2023 Jan;15(3):516.
8. Singh VP, Godara P, Srivastava A. Sustainable microalgal bioremediation of heavy metals and dyes from synthetic wastewater: Progressing towards United Nations Sustainable Development Goals. Waste Manag Bull. 2024 Dec 1;2(4):123–35.
9. Meftah S, Meftah K, Drissi M, Radah I, Malous K, Amahrous A, et al. Heavy metal polluted water: Effects and sustainable treatment solutions using bio-adsorbents aligned with the SDGs. Discov Sustain. 2025 Feb 25;6(1):137.
10. Khan T, Isa MH, Mustafa MRU, Yeek-Chia H, Baloo L, Manan TSBA, et al. Cr(VI) adsorption from aqueous solution by an agricultural waste based carbon. RSC Adv. 2016 June 9;6(61):56365–74.
11. Foo LPY, Tee CZ, Raimy NR, Hassell DG, Lee LY. Potential Malaysia agricultural waste materials for the biosorption of cadmium(II) from aqueous solution. Clean Technol Environ Policy. 2012 Apr 1;14(2):273–80.
12. Khalifa MAS, Malek NANN, Farimani AY, Sani NS, Kamaru AA. Cetylpyridinium bromide (CPB)-treated sugarcane bagasse for the removal of chromate in aqueous solution. Mater Today Proc. 2021 Jan 1;47:1252–7.
13. Garg UK, Kaur MP, Garg VK, Sud D. Removal of hexavalent chromium from aqueous solution by agricultural waste biomass. J Hazard Mater. 2007 Feb 9;140(1–2):60–8.
14. Vijayaraghavan K, Joshi UM, Balasubramanian R. Removal of metal ions from storm-water runoff by low-cost sorbents: Batch and column studies. J Environ Eng. 2010;136(10):1113–8.
15. Mesfin Yeneneh A, Maitra S, Eldemerdash U. Study on biosorption of heavy metals by modified lignocellulosic waste. J Appl Sci. 2011;11(21):3555–62.
16. Dos Santos VCG, Salvado ADPA, Dragunski DC, Peraro DNC, Tarley CRT, Caetano J. Highly improved chromium (III) uptake capacity in modified sugarcane bagasse using different chemical treatments. Quimica Nova. 2012;35(8):1606–11.
17. Ullah I, Nadeem R, Iqbal M, Manzoor Q. Biosorption of chromium onto native and immobilized sugarcane bagasse waste biomass. Ecol Eng. 2013;60:99–107.
18. Sadaf S, Bhatti HN, Nausheen S, Noreen S. Potential use of low-cost lignocellulosic waste for the removal of direct violet 51 from aqueous solution: Equilibrium and breakthrough studies. Arch Environ Contam Toxicol. 2014;66(4):557–71.
19. Mahmood-ul-Hassan M, Suthar V, Rafique E, Ahmad R, Yasin M. Kinetics of cadmium, chromium, and lead sorption onto chemically modified sugarcane bagasse and wheat straw. Environ Monit Assess. 2015 June 27;187(7):470.
20. Tawfik GM, Dila KAS, Mohamed MYF, Tam DNH, Kien ND, Ahmed AM, et al. A step by step guide for conducting a systematic review and meta-analysis with simulation data. Trop Med Health. 2019 Aug 1;47(1):46.
21. Khare KS, Phelan FR. Quantitative Comparison of Atomistic Simulations with Experiment for a Cross-Linked Epoxy: A Specific Volume-Cooling Rate Analysis. Macromolecules. 2018;51(2):564–75.
22. Hannan EJ, Quinn BG. The Determination of the Order of an Autoregression. J R Stat Soc Ser B Methodol. 1979;41(2):190–5.
23. Ross T. Indices for performance evaluation of predictive models in food microbiology. J Appl Bacteriol. 1996;81(5):501–8.
24. Ezekiel M. The Sampling Variability of Linear and Curvilinear Regressions: A First Approximation to the Reliability of the Results Secured by the Graphic 'Successive Approximation' Method. Ann Math Stat. 1930;1(4):275–333.
25. Akaike H. A New Look at the Statistical Model Identification. IEEE Trans Autom Control. 1974;19(6):716–23.
26. Burnham KP, Anderson DR. Multimodel inference: Understanding AIC and BIC in model selection. Sociol Methods Res. 2004;33(2):261–304.
27. Marquardt DW. An Algorithm for Least-Squares Estimation of Nonlinear Parameters. J Soc Ind Appl Math. 1963;11(2):431–41.
28. Seidel A, Gelbin D. On applying the ideal adsorbed solution theory to multicomponent adsorption equilibria of dissolved organic components on activated carbon. Chem Eng Sci. 1988 Jan 1;43(1):79–88.
29. Porter JF, McKay G, Choy KH. The prediction of sorption from a binary mixture of acidic dyes using single- and mixed-isotherm variants of the ideal adsorbed solute theory. Chem Eng Sci. 1999;54(24):5863–85.
30. Schwarz G. Estimating the Dimension of a Model. Ann Stat. 1978;6(2):461–4.
31. Motulsky HJ, Ransnas LA. Fitting curves to data using nonlinear regression: a practical and nonmathematical review. FASEB J. 1987;1(5):365–74.
32. Langmuir I. THE ADSORPTION OF GASES ON PLANE SURFACES OF GLASS, MICA AND PLATINUM. J Am Chem Soc. 1918;40(2):1361–402.

33. Schirmer W. Physical Chemistry of Surfaces. Z Für Phys Chem. 1999;210(1):134–5.
34. Ridha FN, Webley PA. Anomalous Henry's law behavior of nitrogen and carbon dioxide adsorption on alkali-exchanged chabazite zeolites. Sep Purif Technol. 2009;67(3):336–43.
35. Jovanović DS. Physical adsorption of gases - I: Isotherms for monolayer and multilayer adsorption. Kolloid-Z Amp Z Für Polym. 1969;235(1):1203–13.
36. Carmo AM, Hundal LS, Thompson ML. Sorption of hydrophobic organic compounds by soil materials: Application of unit equivalent Freundlich coefficients. Environ Sci Technol. 2000;34(20):4363–9.
37. Radushkevich LV. Potential theory of sorption and structure of carbons. Zhurnal Fiz Khimii. 1949;23:1410–20.
38. Dubinin MM. Modern state of the theory of volume filling of micropore adsorbents during adsorption of gases and steams on carbon adsorbents. Zh Fiz Khim. 1965;39(6):1305–17.
39. Mahanty B, Behera SK, Sahoo NK. Misinterpretation of Dubinin–Radushkevich isotherm and its implications on adsorption parameter estimates. Sep Sci Technol. 2023 May 3;58(7):1275–82.
40. Mudhoo A, Pittman CU. The Dubinin-Radushkevich models: Dissecting the *ps*/*p* to *cs*/*ce* replacement in solid-aqueous interfacial adsorption and tracking the validity of E = 8 kJ mol–1 for assigning sorption type. Chem Eng Res Des. 2023 Oct 1;198:370–402.
41. Koble RA, Corrigan TE. Adsorption isotherms for pure hydrocarbons. Ind Eng Chem. 1952 Feb 1;44(2):383–7.
42. Temkin MI, Pyzhev V. Kinetics of ammonia synthesis on promoted iron catalysts. Acta Physicochim USSR. 1940;12(3):327–56.
43. Chu KH. Revisiting the Temkin Isotherm: Dimensional Inconsistency and Approximate Forms. Ind Eng Chem Res [Internet]. 2021 Aug 16 [cited 2022 Sept 1]; Available from: https://pubs.acs.org/doi/pdf/10.1021/acs.iecr.1c01788
44. Redlich O, Peterson DL. A Useful Adsorption Isotherm. Shell Dev Co Emeryv Calif. 1958;63:1024.
45. Sips R. On the structure of a catalyst surface. J Chem Phys. 1948;16(5):490–5.
46. Tóth J. Uniform interpretation of gas/solid adsorption. Adv Colloid Interface Sci. 1995;55(C):1–239.
47. Hill AV. The possible effects of the aggregation of the molecules of haemoglobin on its dissociation curves. J Physiol. 1910;40:iv–vii.
48. Khan AA, Singh RP. Adsorption thermodynamics of carbofuran on Sn (IV) arsenosilicate in H+, Na+ and Ca2+ forms. Colloids Surf. 1987;24(1):33–42.
49. Brunauer S, Emmett PH, Teller E. Adsorption of Gases in Multimolecular Layers. J Am Chem Soc. 1938;60(2):309–19.
50. Vieth WR, Sladek KJ. A model for diffusion in a glassy polymer. J Colloid Sci. 1965;20(9):1014–33.
51. Radke CJ, Prausnitz JM. Adsorption of Organic Solutes from Dilute Aqueous Solution of Activated Carbon. J Am Chem Soc. 1972;11(4):445–51.
52. Liu Y, Liu YJ. Biosorption isotherms, kinetics and thermodynamics. Sep Purif Technol. 2008;61(3):229–42.
53. Tran HN, Bollinger JC, Lima EC, Juang RS. How to avoid mistakes in treating adsorption isotherm data (liquid and solid phases): Some comments about correctly using Radke-Prausnitz nonlinear model and Langmuir equilibrium constant. J Environ Manage. 2023 Jan 1;325(Pt A):116475.
54. Brouers F, Sotolongo O, Marquez F, Pirard JP. Microporous and heterogeneous surface adsorption isotherms arising from Levy distributions. Phys Stat Mech Its Appl. 2005 Apr 1;349(1):271–82.
55. Hamissa AMB, Brouers F, Mahjoub B, Seffen M. Adsorption of Textile Dyes Using Agave Americana (L.) Fibres: Equilibrium and Kinetics Modelling. Adsorpt Sci Technol. 2007 June 1;25(5):311–25.
56. Brouers F, Al-Musawi TJ. Brouers-Sotolongo fractal kinetics versus fractional derivative kinetics: A new strategy to analyze the pollutants sorption kinetics in porous materials. J Hazard Mater. 2018 May 15;350:162–8.
57. Fritz W, Schluender EU. Simultaneous adsorption equilibria of organic solutes in dilute aqueous solutions on activated carbon. Chem Eng Sci. 1974;29(5):1279–82.
58. Chu KH, Tan B. Is the Frumkin (Fowler–Guggenheim) adsorption isotherm a two- or three-parameter equation? Colloid Interface Sci Commun. 2021 Nov 1;45:100519.
59. Martucci A, Braschi I, Bisio C, Sarti E, Rodeghero E, Bagatin R, et al. Influence of water on the retention of methyl tertiary-butyl ether by high silica ZSM-5 and Y zeolites: A multidisciplinary study on the adsorption from liquid and gas phase. RSC Adv. 2015;5(106):86997–7006.
60. Chu KH, Debord J, Harel M, Bollinger JC. Mirror, Mirror on the Wall, Which Is the Fairest of Them All? Comparing the Hill, Sips, Koble–Corrigan, and Liu Adsorption Isotherms. Ind Eng Chem Res. 2022 May 18;61(19):6781–90.
61. Shukor MY. Chitosan–Silica Composite Aerogel for the Adsorption of Cupric Ions: Isothermal Remodeling and MOORA-Based Model Selection. J Environ Microbiol Toxicol. 2024 Dec 26;12(2):53–62.
62. Karel W, Brauers W, Zavadskas E. The MOORA method and its application to privatization in a transition economy. Control Cybern. 2006 Jan 1;35.
63. Brauers W. Multi-objective seaport planning by MOORA decision making. Ann Oper Res. 2013 July 1;206.
64. Mishra SK. The Most Representative Composite Rank Ordering of Multi-Attribute Objects by the Particle Swarm Optimization [Internet]. Rochester, NY: Social Science Research Network; 2009 [cited 2025 Feb 20]. Available from: https://papers.ssrn.com/abstract=1326386
65. Gupta A, Gupta N, Garg R, Kumar R. Evaluation, Selection and Ranking of Software Reliability Growth Models using Multi criteria Decision making Approach. In: 2018 4th International Conference on Computing Communication and Automation (ICCCA) [Internet]. 2018 [cited 2025 Feb 18]. p. 1–8. Available from: https://ieeexplore.ieee.org/abstract/document/8777644
66. Serafin J, Dziejarski B. Application of isotherms models and error functions in activated carbon CO2 sorption processes. Microporous Mesoporous Mater. 2023 Apr 15;354:112513.
67. Lambert RJW, Mytilinaios I, Maitland L, Brown AM. Monte Carlo simulation of parameter confidence intervals for non-linear regression analysis of biological data using Microsoft Excel. Comput Methods Programs Biomed. 2012 Aug 1;107(2):155–63.
68. Wu Z, Joo H, Ahn IS, Haam S, Kim JH, Lee K. Organic dye adsorption on mesoporous hybrid gels. Chem Eng J. 2004 Sept 15;102(3):277–82.
69. Chandra IK, Ju YH, Ayucitra A, Ismadji S. Evans blue removal from wastewater by rarasaponin-bentonite. Int J Environ Sci Technol. 2013;10(2):359–70.
70. Vijayaraghavan K, Yun YS. Biosorption of C.I. Reactive Black 5 from aqueous solution using acid-treated biomass of brown seaweed Laminaria sp. Dyes Pigments. 2008 Jan 1;76(3):726–32.
71. Foo KY, Hameed BH. Insights into the modeling of adsorption isotherm systems. Chem Eng J. 2010;156(1):2–10.
72. Belhachemi M, Addoun F. Comparative adsorption isotherms and modeling of methylene blue onto activated carbons. Appl Water Sci. 2011 Dec 1;1(3):111–7.
73. Sivarajasekar N, Baskar R. Adsorption of basic red 9 onto activated carbon derived from immature cotton seeds: isotherm studies and error analysis. Desalination Water Treat. 2014 Dec 6;52(40–42):7743–65.
74. Ayawei N, Ebelegi AN, Wankasi D. Modelling and Interpretation of Adsorption Isotherms. J Chem. 2017 Sept 5;2017:e3039817.
75. Maaloul N, Oulego P, Rendueles M, Ghorbal A, Díaz M. Cu(II) Ions Removal on Functionalized Cellulose Beads from Tunisian Almond (Prunus dulcis) Shell. Environ Sci Eng. 2021;65–71.
76. Langmuir I. The constitution and fundamental properties of solids and liquids. Part I. Solids. J Am Chem Soc. 1916;38(11):2221–95.
77. Karnib M, Kabbani A, Holail H, Olama Z. Heavy Metals Removal Using Activated Carbon, Silica and Silica Activated Carbon Composite. Energy Procedia. 2014 Dec 31;50:113–20.
78. Hyder AHMG, Begum SA, Egiebor NO. Adsorption isotherm and kinetic studies of hexavalent chromium removal from aqueous solution onto bone char. J Environ Chem Eng. 2015 June 1;3(2):1329–36.
79. Divband Hafshejani L, Mortazavi P, Sabz ALiPour S, Brooman Nasab S. Isotherm and Kinetics Study of The Adsorption of Chromium (VI) From Aqueous Solution by Zizyphus Spina-christi Leaves Ash Nanoparticles. Irrig Sci Eng. 2016 Dec 21;39(4):97–110.
80. Taha AA, Shreadah MA, Ahmed AM, Heiba HF. Multi-component adsorption of Pb(II), Cd(II), and Ni(II) onto Egyptian Na-activated

bentonite; Equilibrium, kinetics, thermodynamics, and application for seawater desalination. J Environ Chem Eng. 2016;4(1):1166–80.
81. Nag S, Mondal A, Bar N, Das SK. Biosorption of chromium (VI) from aqueous solutions and ANN modelling. Environ Sci Pollut Res. 2017 Aug 1;24(23):18817–35.
82. Srivastava S, Agrawal SB, Mondal MK. Synthesis, characterization and application of Lagerstroemia speciosa embedded magnetic nanoparticle for Cr(VI) adsorption from aqueous solution. J Environ Sci China. 2017 May;55:283–93.
83. Ahsan MdA, Jabbari V, Islam MdT, Kim H, Hernandez-Viezcas JA, Lin Y, et al. Green synthesis of a highly efficient biosorbent for organic, pharmaceutical, and heavy metal pollutants removal: Engineering surface chemistry of polymeric biomass of spent coffee waste. J Water Process Eng. 2018 Oct 1;25:309–19.
84. Boeykens SP, Saralegui A, Caracciolo N, Piol MN. Agroindustrial waste for lead and chromium biosorption. J Sustain Dev Energy Water Environ Syst. 2018;6(2):341–50.
85. Mahmood-Ul-Hassan M, Suthar V, Ahmad R, Yousra M. Biosorption of metal ions on lignocellulosic materials: batch and continuous-flow process studies. Environ Monit Assess. 2018;190(5).
86. Mortazavian S, An H, Chun D, Moon J. Activated carbon impregnated by zero-valent iron nanoparticles (AC/nZVI) optimized for simultaneous adsorption and reduction of aqueous hexavalent chromium: Material characterizations and kinetic studies. Chem Eng J. 2018 July 1;353.
87. Sadiq A, Choubey A, Bajpai AK, Sadiq A, Choubey A, Bajpai AK. Biosorption of chromium ions by calcium alginate nanoparticles. J Chil Chem Soc. 2018;63(3):4077–81.
88. Abilio TE, Soares BC, José JC, Milani PA, Labuto G, Carrilho ENVM. Hexavalent chromium removal from water: adsorption properties of in natura and magnetic nanomodified sugarcane bagasse. Environ Sci Pollut Res. 2021;28(19):24816–29.
89. Dan-Iya BI, Shukor MY. Isothermal Modelling of the Adsorption of Chromium onto Calcium Alginate Nanoparticles. J Environ Microbiol Toxicol. 2021 Dec 31;9(2):1–7.
90. Mahmoud ME, El-Said GF, Ibrahim GAA, Elnashar AAS. Effective removal of hexavalent chromium from water by sustainable nano-scaled waste avocado seeds: adsorption isotherm, thermodynamics, kinetics, and error function. Biomass Convers Biorefinery [Internet]. 2022; Available from: https://www.scopus.com/inward/record.uri?eid=2-s2.0-85144861871&doi=10.1007%2fs13399-022-03619-2&partnerID=40&md5=92f885dfde215c605d5baa0cebf9b79c
91. Freundlich H. Über die adsorption in lösungen (Over the adsorption in solution). Z Für Phys Chem. 1907;57(1):385–470.
92. Rushton G, Karns C, Shimizu K. A critical examination of the use of the Freundlich isotherm in characterizing molecularly imprinted polymers (MIPs). Anal Chim Acta. 2005 Jan 3;528:107–13.
93. Ahmed S, Guo Y, Li D, Tang P, Feng Y. Superb removal capacity of hierarchically porous magnesium oxide for phosphate and methyl orange. Environ Sci Pollut Res. 2018 Sept 1;25(25):24907–16.